Cerebral Cortex February 2013;23:293–304
doi:10.1093/cercor/bhs006
Advance Access publication February 7, 2012

Interpyramid Spike Transmission Stabilizes the Sparseness of Recurrent Network Activity

Yuji Ikegaya, Takuya Sasaki, Daisuke Ishikawa, Naoko Honma, Kentaro Tao, Naoya Takahashi, Genki Minamisawa, Sakiko Ujita and Norio Matsuki

Laboratory of Chemical Pharmacology, Graduate School of Pharmaceutical Sciences, The University of Tokyo, Tokyo 113-0033, Japan

Yuji Ikegaya, Takuya Sasaki, Daisuke Ishikawa, and Naoko Honma contributed equally to this work.

Address correspondence to email: ikegaya@mol.f.u-tokyo.ac.jp.

Cortical synaptic strengths vary substantially from synapse to synapse and exhibit a skewed distribution with a small fraction of synapses generating extremely large depolarizations. Using multiple whole-cell recordings from rat hippocampal CA3 pyramidal cells, we found that the amplitude of unitary excitatory postsynaptic conductances approximates a lognormal distribution and that in the presence of synaptic background noise, the strongest fraction of synapses could trigger action potentials in postsynaptic neurons even with single presynaptic action potentials, a phenomenon termed interpyramid spike transmission (IpST). The IpST probability reached 80%, depending on the network state. To examine how IpST impacts network dynamics, we simulated a recurrent neural network embedded with a few potent synapses. This network, unlike many classical neural networks, exhibited distinctive behaviors resembling cortical network activity in vivo. These behaviors included the following: 1) infrequent ongoing activity, 2) firing rates of individual neurons approximating a lognormal distribution, 3) asynchronous spikes among neurons, 4) net balance between excitation and inhibition, 5) network activity patterns that was robust against external perturbation, 6) responsiveness even to a single spike of a single excitatory neuron, and 7) precise firing sequences. Thus, IpST captures a surprising number of recent experimental findings in vivo. We propose that an unequally biased distribution with a few select strong synapses helps stabilize sparse neuronal activity, thereby reducing the total spiking cost, enhancing the circuit responsiveness, and ensuring reliable information transfer.

Keywords: action potential, hippocampus, lognormal distribution, spike information, synaptic efficacy, synaptic potency, synaptic transmission, neocortex, pyramidal cell

Introduction

As cortical excitatory synapses are weak and stochastic, a neuron cannot fire an action potential unless it receives a number of synaptic inputs in a narrow time window. This integrate-and-fire schema naturally leads to the "synfire chain" hypothesis, in which stable spike propagation to downstream network layers requires synchronization among presynaptic neuron groups (Abeles 1991; Diesmann et al. 1999; Reyes 2003); however, this synchrony-based signal propagation is challenged by 2 recent findings.

First, spontaneous spiking by the majority of cortical neurons in vivo is infrequent, usually with a frequency of less than 1 Hz (Margrie et al. 2002; O'Connor et al. 2010; Minamisawa et al. 2011), and highly asynchronous (Ecker et al. 2010; Renart et al. 2010). The sparseness of neuronal activity is practical in terms of signal detection (Ecker et al. 2010) and energy consumption (Lennie 2003), but intuitively, such highly sporadic activity must eventually reach a point of no activity because it cannot depolarize postsynaptic neurons to their spike threshold. Thus, how cortical networks can maintain asynchronous and infrequent activity is enigmatic.

Second, the effects of single neurons on the network dynamics are unexpectedly strong. An early report indicated that single CA3 pyramidal cells (PCs) can initiate synchronized rhythmic burst discharges in disinhibited hippocampal slices (Miles and Wong 1983). We more recently demonstrated that the stimulation of single CA3 PCs can initiate a transition of the network firing state in hippocampal slice cultures (Fujisawa et al. 2006). In vivo studies appear consistent with these findings. Addition of a single extraspike to ongoing cortical activity results in a transient increase in the firing rates of surrounding neurons (London et al. 2010). More surprisingly, single PC stimulation is capable of switching the up/down state of the entire brain in anesthetized rats (Li et al. 2009), and spike trains evoked in a single somatosensory PC can evoke whisker movements or behavioral responses (Brecht et al. 2004; Houweling and Brecht 2008). These results indicate that nonsynchronized PC activity can propagate in noisy cortical network.

These observations cannot be explained by the classic spike propagation model. To reconcile the apparent contradictions, we focused on recent literature concerning the distribution of unitary synaptic weights among neocortical PCs, where a small fraction of PC pairs generate extremely large synaptic potentials, the amplitudes of which occasionally reach nearly 10 mV (roughly corresponding to 2 nS) (Song et al. 2005; Lefort et al. 2009). Because the outliers are 1 or 2 orders of magnitude stronger than common PC synapses, we hypothesized that they can reliably elicit spikes in the postsynaptic PCs and that this phenomenon, termed interpyramid spike transmission (IpST), can thereby stabilize sparse spiking and augment the power of single neurons.

Materials and Methods

The experiments were performed with the approval of the animal experiment ethics committee at the University of Tokyo (approval numbers: 19–41, 19–43) and according to the University of Tokyo guidelines for the care and use of laboratory animals. Data are reported as the means ± standard deviations (SDs).

Ex Vivo experiments

Postnatal day 7 Wistar/ST rats of either sex were chilled with ice and decapitated. The brains were removed and cut horizontally using a Dosaka DTK-1500 vibratome into 300-μm thick slices in aerated ice-cold Gey's balanced salt solution supplemented with 25 mM glucose. Entorhino-hippocampal stumps were cultivated on Omnipore membrane filters (JHWP02500, φ25 mm; Millipore) (Koyama et al. 2007).

Cultures were fed with 50% minimal essential medium, 25% Hank's balanced salt solution (Invitrogen, Carlsbad, CA), and 25% horse serum (Cell Culture Laboratory, Cleveland, OH) in a humidified incubator at 37 °C in 5% CO_2. The medium was changed every 3.5 days. Experiments were performed at 7–10 days in vitro. Slices were placed in a recording chamber and perfused at a rate of 1.5–2 mL/min with artificial cerebrospinal fluid (aCSF) that consisted of (in mM) 123 NaCl, 26 $NaHCO_3$, 2.2 KCl, 1.24 NaH_2PO_4, 2.0 $MgSO_4$, 2.0 $CaCl_2$, and 10 glucose (32 °C), and they were bubbled with 95% O_2/5% CO_2. CA3 PCs were visually identified and randomly selected for patch-clamp recordings using infrared differential interference contrast microscopy. Borosilicate glass pipettes (5–9 MΩ) were filled with an internal solution that consisted of (in mM) 135 K-gluconate, 4 KCl, 10 4-(2-hydroxyethyl)-1-piperazineethanesulfonic acid, 0.2 ethyleneglycol-bis(2-aminoethylether)-N,N,N',N'-tetra acetic acid, 10 phosphocreatine-Na_2, 0.3 Na_2-GTP, 4 Mg-ATP, and 2 mg/mL biocytin (pH 7.2). Whole-cell recordings were collected at 20 kHz and filtered at 10 kHz using 2 MultiClamp 700B amplifiers and a Digidata 1440A digitizer that were controlled by pCLAMP 10 software (Molecular Devices). To measure the amplitude (the so-called "potency") of unitary excitatory postsynaptic conductances (uEPSGs; failure transmission trials omitted), depolarizing currents were injected repeatedly (50–100 times) into presynaptic neurons to induce single action potentials, and the evoked uEPSGs were monitored at a holding voltage of −70 mV. The uEPSG amplitude was estimated as the peak amplitude of an evoked postsynaptic current by −70 mV and was represented in nS. To evaluate the efficiency of IpST, Gaussian background noise (σ = 200 pA) was continuously injected into postsynaptic neurons, and the postsynaptic neurons were activated by single presynaptic action potentials. IpST was defined as any postsynaptic spike occurring between 1 and 30 ms after a given presynaptic spike. The IpST probability was calculated as $(N_{IpST} - N_{chance})/(N_{total} - N_{chance})$, where N_{total} is the total number of spikes evoked in the presynaptic neuron (i.e., all trials), N_{IpST} is the number of postsynaptic spikes time locked to the evoked presynaptic spikes (i.e., apparent IpST trials), and N_{chance} is the number of "chance" IpST. N_{chance} was predicted by a Poissonian stochastic process based on the background firing rate of the postsynaptic neuron. The P value for the IpST probability was obtained by a Z-test for proportion (binomial distribution) (Kendall et al. 1994). Specifically, we considered a random sample of N_{total} taken from a population in which a proportion R_0 belongs to the spontaneous background (here, we assumed $R_0 = N_{chance}/N_{total}$). The null hypothesis that the proportion R (N_{IpST}/N_{total}) is equal to R_0 was statistically tested based on the test statistic $Z = (|R - R_0| - 0.5 \times N_{total})/[R_0 (1 - R_0)/N_{total}]^{1/2}$.

The Z value was compared with a standard normal distribution using a two-tailed test. For high-speed functional multineuron calcium imaging (fMCI) (Takahashi et al. 2011), slices were incubated with 2 mL of dye solution at 37 °C for 1 h. The dye solution was aCSF containing 0.0005% Oregon Green 488 BAPTA-1 AM (Invitrogen), 0.01% Pluronic F-127 (Invitrogen), and 0.005% Cremophor EL (Invitrogen). After 1 h of recovery, the slices were transferred into a recording chamber perfused with aCSF modified to enhance the level of spontaneous activity (Sanchez-Vives and McCormick 2000; Takahashi et al. 2010). The modified aCSF consisted of (in mM) 127 NaCl, 26 $NaHCO_3$, 3.3 KCl, 1.24 KH_2PO_4, 1.0 $MgSO_4$, 1.0–1.2 $CaCl_2$, and 10 glucose. Images were acquired from a CA3 PC layer at 500 frames per second with a Nipkow-disk confocal unit (CSU-X1, Yokogawa Electric, Tokyo, Japan), a back-illuminated CCD camera (iXon DU860, Andor, Belfast, Northern Ireland, UK), a water-immersion objective lens (16×, 0.80 NA, Nikon, Tokyo, Japan), and Solis software (Andor). Fluorophores were excited at 488 nm and visualized with a 507-nm long-pass emission filter. In each cell body, the fluorescence change $\Delta F/F$ was calculated as $(F_t - F_0)/F_0$, where F_t is the fluorescence intensity at frame time t and F_0 is the baseline. Spike timing was determined at the onset of a Ca^{2+} transient with an automatic machine-learning algorithm that can accurately detect the timing within one-frame jitter error (Sasaki et al. 2008).

In Toto experiments

Postnatal 12- to 14-day-old male Wistar/ST rats were anesthetized with ether and decapitated. The brains were quickly removed and immersed in ice-cold sucrose-based aCSF consisting of (in mM) 27 $NaHCO_3$, 1.4 NaH_2PO_4, 2.5 KCl, 7.0 $MgSO_4$, 1.0 $CaCl_2$, 222 sucrose, and 0.5 ascorbic acid, and they were bubbled with 95% O_2 and 5% CO_2. The hippocampal formations were surgically isolated from the surrounding brain structures, transferred into oxygenated aCSF that consisted of (in mM) 126 NaCl, 24.0 $NaHCO_3$, 4.0 KCl, 2.0 $MgSO_4$, 1.24 NaH_2PO_4, 2.0 $CaCl_2$, and 10 glucose, and maintained at room temperature for at least 45 min. The hippocampal tissue was submerged in a chamber, perfused with oxygenated aCSF at a rate of 10–15 mL/min at 30–32 °C, and fixed to a silicon bottom with 4–6 thin entomological needles so that the CA3 surface became the top side of the preparation. CA3 PCs were targeted for whole-cell recordings under visually controlled infrared differential interference contrast microscopy. To record local field potentials (LFPs), another glass pipette (1–2 MΩ) filled with aCSF was inserted into the CA3 PC layer 200–400 μm away from the patched neuron. The patched PCs were stimulated with the dynamic-clamp conductance injection technique (Takahashi et al. 2010). Synaptic event models were based on conductance $g(t)$, and the command current signal $I(t)$ was computed as $I(t) = g(t) \times (V(t) - E_{rev})$ ($V(t)$: membrane potential at time t; E_{rev}: reversal potential = 0 mV) under a real-time Linux environment and delivered into patch-clamped neurons at 20 kHz using a PCI-6024E data acquisition board (National Instruments). The conductance stimulus consisted of excitatory synaptic inputs mediated by α-amino-3-hydroxy-5-methyl-4-isoxazolepropionic acid (AMPA) and *N*-methyl-D-aspartate (NMDA) receptors, and it was fitted by the dual exponential function $(g_0 \times (e^{-t/\tau_1} - e^{-t/\tau_2})$, where τ_1 represents an activation time constant, τ_2 is a decay time constant, and g_0 is a scaling factor (τ_1 = 1 ms, τ_2 = 8 ms for AMPA receptors, τ_1 = 3 ms, and τ_2 = 300 ms for NMDA receptors). The voltage-dependent release of magnesium blockage in NMDA receptor conductances was modeled as:

$$1/\left(1 + \left([Mg^{2+}]_o/3.57\right) \times e^{-0.062 \times V(t)}\right), \quad (1)$$

where $[Mg^{2+}]_o$ was the external magnesium concentration of 1 mM (Jahr and Stevens 1990). After the completion of the physiological measurements, the type of neuron recorded was confirmed by biocytin staining. After overnight fixation with 4% paraformaldehyde, the hippocampus was sliced at a thickness of 100 μm using a vibratome and then incubated at room temperature with 0.3% Triton-X100 for 6 h followed by Alexa Fluor 488-conjugated streptavidin (1:500; S32354, Invitrogen) for 6 h. Biocytin-positive neurons were microscopically identified and visualized with a BioRad MRC-1000 laser scanning confocal system. Only data obtained from PCs were used for analysis.

In Silico experiments

All model neurons obeyed the leaky integrate-and-fire model (Dayan and Abbott 2001). Our recurrent network consisted of 4000 excitatory and 1000 inhibitory neurons, and all excitatory and inhibitory neurons were randomly interlinked. The connectivity between all types of synapses was set to be 10%, unless otherwise specified. Each integrate-and-fire neuron was characterized by leak conductance g_{leak} = 4.5 nS, membrane capacitance C = 100 pF, and resting potential V_{rest} = −70 mV. Whenever the membrane potential $V(t)$ crossed a spiking threshold of −55 mV, an action potential was generated, and the membrane potential was reset to V_{rest}, where it remained clamped for refractory periods of 25–40 ms for excitatory neurons and 2–4 ms for inhibitory neurons. $V(t)$ obeyed the following equation:

$$C\frac{dV(t)}{dt} = -g_{leak}(V(t) - V_{rest}) - I_{syn}(t), \quad (2)$$

where $I_{syn}(t)$ is the instantaneous synaptic current and is defined as $I_{syn}(t) = g(t)\,(V(t) - E_{rev})$. E_{rev} is the reversal potential. The function $g(t)$ is the synaptic conductance mediated by either AMPA/NMDA receptors or γ-aminobutyric acid type-A ($GABA_A$) receptors and designed with the double exponential kinetic:

$$g(t) = g_0\left(e^{-(t - t_0 - D)/\tau_2} - e^{-(t - t_0 - D)/\tau_1}\right), \quad (3)$$

where τ_1 and τ_2 are the rise and decay time constants, t_0 is the time when the action potential is generated, and D is the synaptic delay. For the AMPA receptor component, E_{rev} = 0 mV, τ_1 = 1 ms, τ_2 = 8 ms, and D = 1 ms, whereas for the NMDA receptor component, E_{syn} = 0 mV,

τ_1 = 3 ms, τ_2 = 300 ms, and D = 1 ms; $GABA_A$ receptor component: E_{syn} = −80 mV, τ_1 = 1 ms, τ_2 = 8 ms, and D = 2 ms. The quantal conductance g_0 of the AMPA receptors followed a lognormal distribution with the mean $\mu = 10^{-0.31}$ nS and SD $\sigma = 10^{-0.30}$ nS, unless otherwise specified. These g_0 values were further subject to trial-to-trial fluctuations (see below). The NMDA:AMPA conductance ratio was fixed at 1:1, and the magnesium block was modeled as in equation (1), where $[Mg^{2+}]$ was 1 mM (Jahr and Stevens 1990). The conductance of AMPA receptors in the inhibitory neurons was g_0 = 1 nS, that of the GABA receptors in excitatory neurons was g_0 = 4 nS, and that of the GABA receptors in inhibitory neurons was g_0 = 5 nS. Short-term synaptic plasticity was incorporated into all synapses according to previous studies (Markram et al. 1998; Liu and Buonomano 2009), in which the synaptic response generated by the n^{th} action potential in a train was defined as:

$$g_n = g \cdot R_n \cdot u_n \quad (4)$$

R_1 after the first action potential is:

$$R_1 = 1 - U \quad (5)$$

R_n for consecutive action potentials in the train is:

$$R_{n+1} = R_n(1 - u_{n+1})\exp\left(-\frac{\Delta t}{\tau_{rec}}\right) + 1 - \exp\left(-\frac{\Delta t}{\tau_{rec}}\right) \quad (6)$$

$$u_{n+1} = u_n \exp\left(-\frac{\Delta t}{\tau_{facil}}\right) + U\left(1 - u_n \exp\left(-\frac{\Delta t}{\tau_{facil}}\right)\right) \quad (7)$$

Specifically, in the glutamatergic synapses U = 0.5, τ_{rec} = 500 ms, τ_{facil} = 10 ms; in GABAergic synapses, U = 0.25, τ_{rec} = 700 ms, τ_{facil} = 20 ms. The trial-to-trial fluctuation of the synaptic conductance g_0 and the release probability were provided with excitatory neurons, based on the parameters obtained with a least-square fit to our experimental data ex vivo (Fig. 1*G*). The trial-to-trial fluctuation of the synaptic conductance was incorporated into excitatory-to-excitatory synapses. The coefficient of variation (CV) of the synaptic weights was 0.22 × $g_0^{-0.5}$ nS (Fig. 1*G*, green line). At each arrival of a presynaptic action potential, the peak conductance was chosen according to a Gaussian distribution with $\mu = g_0$ and $\sigma = g_0 \times$ CV. No trial-to-trial fluctuations were given to all other types of synapses. The release probability of glutamatergic synapses in excitatory neurons was $1 - e^{-12.3 \times g_0}$ (Fig. 1*G*, blue line). At each arrival of a presynaptic action potential, excitatory-to-excitatory synaptic transmission occurred stochastically with this probability. If the transmission failed, no synaptic conductance was added to the postsynaptic neurons. The release probability at all other types of synapses was 1. The periods of 10–120 min were simulated at a time step of 0.1–0.5 ms. In this range, the time step did not affect the results. The simulation was repeated 10–20 times with different random seeds of connectivity and synaptic weights, producing consistent results. The simulation software was written in MATLAB and executed on a Quad-core 3.2 GHz × 2 CPU personal computer.

Results

Distribution of Interpyramid Synaptic Weights

Using hippocampal slice cultures, whole-cell recordings were performed on 1048 pairs of CA3 PCs to measure synaptic potency, defined as the mean amplitude of uEPSGs across trials with successful synaptic transmission. Depolarizing currents were injected 50–100 times every 10–30 s into presynaptic neurons to induce single action potentials, and the evoked uEPSGs were monitored at a holding voltage of −70 mV. The distribution of uEPSG potency featured a heavy tail generated by a small fraction of large uEPSGs (Fig. 1*A*) and approximated a lognormal distribution (Fig. 1*B*; R = 0.49, $P < 0.0001$). Similar lognormal distributions have been reported in PC-to-PC synaptic weights in acute neocortical slices (Song et al. 2005; Sarid et al. 2007). In our data, the Gini coefficient was 0.49 in the Lorenz curve, which plots the proportion of the distribution assumed by the weakest proportion of the uEPSG

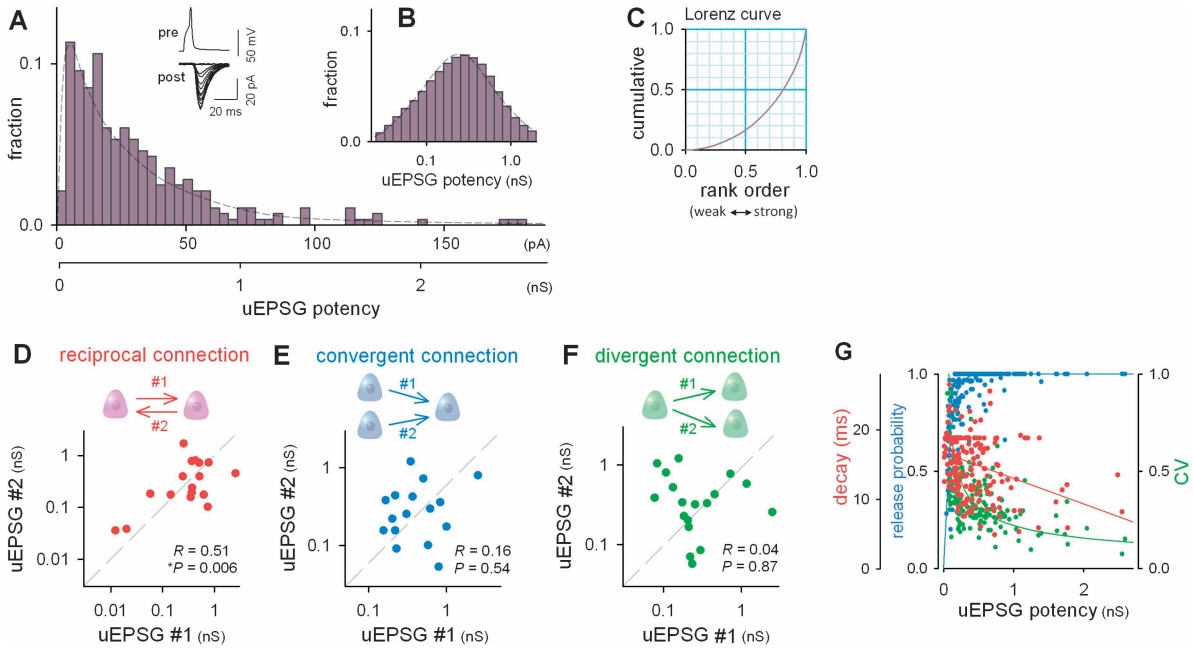

Figure 1. Long-tailed distribution of uEPSGs at CA3-to-CA3 synapses in hippocampal slice cultures. (*A–C*) Normal (*A*), semilog (*B*), and Lorenz (*C*) plots of the distribution in uEPSG potency of 1048 CA3 PC pairs. The uEPSG size was estimated by dividing the peak synaptic current by −70 mV. The broken line indicates the least-square best fit for the lognormal distribution with ($\mu = 10^{-0.31}$ μS, $\sigma = 10^{-0.30}$ μS, R = 0.49, $P < 0.0001$). This distribution gives μ = 0.47 nS and σ = 0.44 nS in linear scale calculation. The inset in *A* indicates a presynaptic spike and 30 trials of postsynaptic responses. (*D–F*) Relationship in uEPSG potency between 2 connections (#1 and #2) in reciprocal 2-cell motifs (*D*), convergent 3-cell motifs (*E*), and divergent 3-cell motifs (*F*). (*G*) The time constant of uEPSG decay (red), the release probability (blue), and the CV of successful trial uEPSG sizes (green) are plotted against the uEPSG potency (g_0). Lines are the least-square fits: decay = $16.7 - 3.7 \times g_0$ (red, R = 0.32, $P < 0.0001$), probability = $1 - e^{-12.3g_0}$ (blue, R = 0.71, $P < 0.0001$), and CV = $0.22 \times g_0^{-0.5}$ (green, R = 0.45, $P < 0.0001$).

potency (Fig. 1C). Specifically, the weakest half contributed only 17% of the total uEPSGs, whereas the strongest 20% contributed 52%. When postsynaptic PCs were current clamped, the largest fraction of uEPSGs elicited depolarizations of up to 10 mV. In microcircuit motifs, uEPSG potency correlated positively with reciprocal connections made by 2 PCs, but not with 2 convergent or divergent connections made by 3 PCs (Fig. 1*D–F*).

The extremely large uEPSGs can be explained by 3 plausible (not exclusive) mechanisms. First, the large uEPSGs could be generated by structurally large synapses. The size of dendritic spines correlates with synaptic strengths (Matsuzaki et al. 2001) and is lognormally distributed (Loewenstein et al. 2011). Second, the large uEPSGs could occur at dendrites proximal to the soma. Indeed, larger uEPSGs had faster waveform kinetics, consistent with cable theory (Fig. 1*G*; red line). Finally, large uEPSGs could arise from multiple synaptic sites (Sorra and Harris 1993; Markram et al. 1997). This idea is consistent with the central limit theorem in large-sample statistics in terms of 2 observations: 1) the probability of transmission failure decreased as a single exponential function e^{-g_0}, where g_0 is the uEPSG potency and is thus roughly proportional to the number of synaptic release sites (Fig. 1*G*; blue line) and 2) CV of the trial-to-trial fluctuations in successful-trial uEPSG sizes was inversely proportional to the root square of g_0 (Fig. 1*G*; green line). Therefore, we think that all these 3 mechanisms could contribute to the generation of large uEPSGs, although we cannot determine the ratios of these contributions, which may affect the distribution shape in synaptic weights.

Interpyramid Spike Transmission (IpST)

Fluctuating currents (Gaussian noise with σ = 200 pA) were continuously injected into a current-clamped postsynaptic PC, and the presynaptic PC was made to fire a single action potential. In strongly connected pairs, the postsynaptic PCs responded with single spikes that were time locked to the presynaptic spikes (Fig. 2*A*), whereas weak synaptic pairs did not exhibit an increase in the firing rate of the postsynaptic neurons (Fig. 2*B*). Because the increased firing rate persisted for 30 ms after presynaptic stimulation (Fig. 2*A*), we defined IpST as a postsynaptic spike occurring between 1 and 30 ms after an evoked presynaptic spike and computed the IpST probability as $(N_{IpST} - N_{chance})/(N_{total} - N_{chance})$, where N_{total} is the total trial number, N_{IpST} is the number of trials that showed IpST, and N_{chance} is the false-positive chance number expected by the background firing rate of the postsynaptic PC. Larger uEPSG potencies generated higher IpST probabilities (Fig. 2*C*, top). We then computed the *P* value for the IpST probability based on the *Z*-test for a proportion (Kendall et al. 1994). IpST that occurred with a significantly high probability was evident for uEPSG potencies of more than about 1 nS (Fig. 2*C*, bottom).

To investigate IpST under conditions of physiological noise, we used in toto hippocampal preparations (Fig. 3*A*), which are known to self-generate theta oscillations typical of hippocampal networks in vivo (Goutagny et al. 2009). In these preparations, CA3 PCs exhibited spontaneous spikes at frequencies of 0.1–2.0 Hz even without noise current injection. Using the dynamic-clamp technique, we injected a uEPSG-shaped conductance (Fig. 3*B*). Larger conductance injections more reliably evoked action potentials. The "apparent" IpST was significant at more than about 1 nS (Fig. 3*C*). CA3 networks alternated spontaneously between theta and nontheta states, spending 32 ± 22% of the observation period in the theta state. In the theta state, the resting membrane potential recorded in CA3 PCs was depolarized by 2.6 ± 0.7 mV (n = 6 neurons). Intermittent sharp waves were observed in the nontheta state. The IpST probabilities were compared between theta and nontheta states using simultaneous recordings of LFPs from the CA3 PC layer. We found that IpST occurred more reliably in the theta-oscillation state (Fig. 3*C* inset, 1 nS, P = 0.01, t_6 = 3.56, paired t-test). Thus, the IpST efficiency is subject to state-dependent modulation, probably through changes in the intrinsic activity of the CA3 network.

To examine whether IpST could be detected in spontaneous network activity, we returned to slice culture preparations and conducted high-speed fMCI from the CA3 PC layer (Takahashi et al. 2010). Transient calcium increases in the somata, reflecting action potentials, were monitored at 500 Hz from 85 ± 25 neurons per slice (n = 14 slices, 53–137 neurons monitored per slice). We defined a delayed event pair (DEP), which may result at least in part from IpST, as any calcium event that occurred in one neuron within 1–30 ms after an event in another neuron. We observed more DEPs in the original data sets than would be expected in random surrogates (Fig. 4*A*). The surrogates were generated by random shuffling of interevent intervals, in which the time intervals between 2 successive calcium activities were transposed at random within each neuron to collapse the temporal correlation between neurons without changing the activity level of individual neurons (Sasaki et al. 2007). The *P* value matrix for these DEPs revealed that significant DEPs occurred between a few neuron pairs (Fig. 4*B–D*). Consistent with the data of Figure 1*D*, reciprocal *P* values in pairs were significantly correlated (Fig. 4*E*, R = 0.84, P < 0.0001). Indeed,

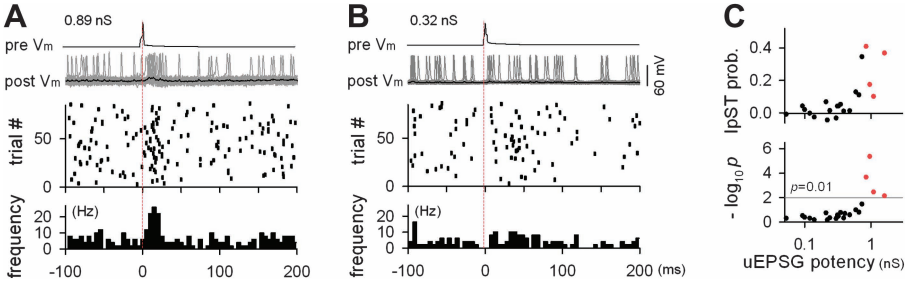

Figure 2. Experimental evidence for IpST in hippocampal slice cultures. (*A*,*B*) Responses of a postsynaptic PC to single spikes from a presynaptic PC that produced uEPSGs with a potency of 0.89 nS (*A*) and 0.32 nS (*B*). Top: traces of a representative presynaptic spike (evoked at time 0) and 20 randomly selected postsynaptic voltage responses. Middle: rastergram of postsynaptic spikes. Bottom: peri-presynaptic spike time histogram of postsynaptic spikes. (*C*) IpST probability and *P* values are plotted against the uEPSG potency. Each dot indicates a single cell pair. Red dots are $P < 0.01$. $n = 20$ pairs.

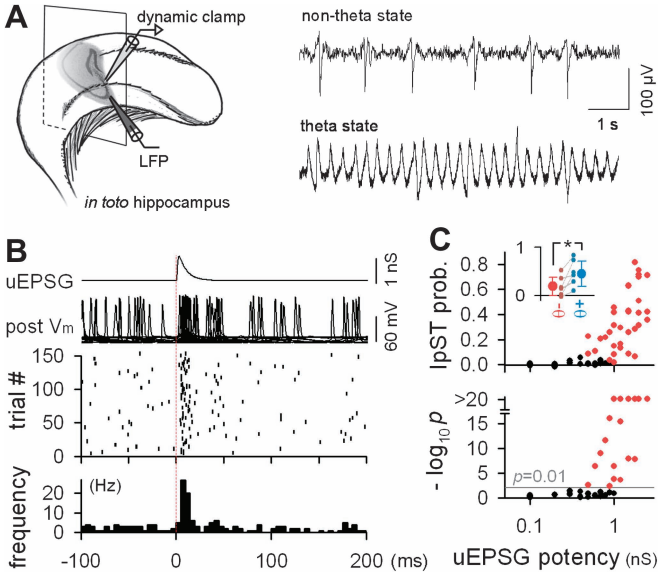

Figure 3. State-dependent IpST in intact hippocampal preparations. (*A*) LFP of the CA3 PC layer in an in toto hippocampal preparation were recorded during dynamic-clamp experiments. CA3 networks alternated spontaneously between theta and nontheta states. (*B*) Spikes evoked by dynamic-clamp injection of uEPSG-like conductance (1 nS) into a CA3 PC. (*C*) Data obtained from 7 PCs. Red dots indicate $P < 0.01$. The IpST probability (uEPSG-like conductance = 1 nS) in nontheta and theta states was separately plotted in the inset ($P = 0.01$, $t_6 = 3.56$, paired *t*-test).

we encountered bidirectional chains of multiple DEPs during network synchronizations (Fig. 4*F*), which resemble the forward and reverse replay of hippocampal place cell activity during sharp-wave ripple complexes (Lee and Wilson 2002; Foster and Wilson 2006; Diba and Buzsaki 2007); note that we previously demonstrated that these CA3 synchronizations are associated with sharp-wave ripples in LFPs (Takahashi et al. 2010).

Self-Sustained Spiking Activity in a Network Embedded with a Few Strong Synapses

Based on our electrophysiological data ex vivo, we simulated a recurrent neural network model. Our network included 5000 leaky integrate-and-fire units consisting of 4000 excitatory and 1000 inhibitory neurons. The 5000 neurons were randomly linked with a connectivity of 10%. The network size and the connection sparsity were nearly identical to those of the hippocampal CA3 recurrent network ex vivo (Takahashi et al. 2010; Kimura et al. 2011). The excitatory-to-excitatory synapses were lognormally distributed in weight and were given stochastic transmission and trial-to-trial fluctuations as shown in Figure 1*G*. We did not consider dendritic computation because we collected the uEPSG distribution from the cell body (Fig. 1*A*).

Initially, a small percentage of neurons were randomly selected from the 4000 excitatory neurons, and these neurons were made to fire single action potentials. Surprisingly, these initial spikes were autonomously amplified and maintained at an apparently steady level even without further external inputs or additional spikes (Fig. 5*A*). This phenomenon is not trivial because neural networks in which synaptic weights conform to Gaussian or homogenous distributions usually require continuous driving noise to maintain spiking activity (data not shown, see also Fig. 6). We therefore analyzed this characteristic self-sustained activity. Consequently, we found that the activity

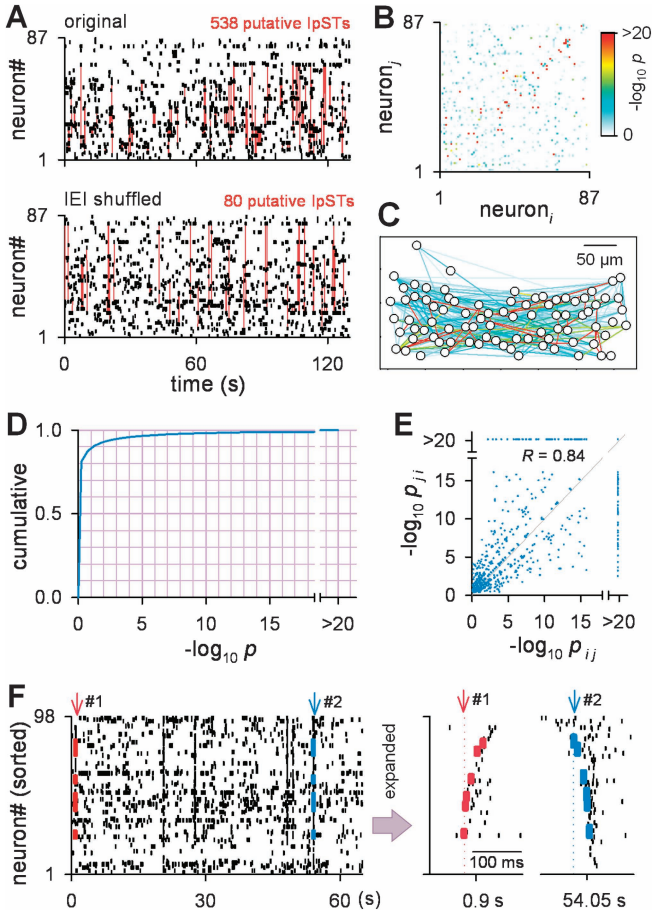

Figure 4. Spike sequences in spontaneously active networks of hippocampal slice cultures. The spiking activity of CA3 neurons was recorded at 500 frames per second using fMCI. (*A*) Spatiotemporal patterns (rastergram) of spontaneous spike activity. Each black dot indicates the timing of a single action potential–evoked calcium event. Red lines indicate DEPs detected in a rastergram (top) and its surrogate (bottom). The surrogate was generated by random shuffling of interevent time intervals (IEI shuffled). The number of DEPs was reduced in the surrogate. The same result was obtained in all 1000 surrogates. (*B*) Matrix of the *P* values for DEPs observed in all neuron pairs of the rastergram shown in (*A*). (*C*) Cell-map representation of the *P* value matrix. (*D*) Cumulative *P* value distribution. $n = 108\,478$ pairs in 14 slices. (*E*) *P* values were reciprocally correlated between 2 neurons *i* and *j* ($R = 0.84$, $P < 0.0001$). (*F*) Example of forward and reverse spike sequences consisting of 5 DEPs, which are indicated by colored dots and magnified in the right panels.

1) was spatiotemporally sparse, 2) maintained the balance between excitation and inhibition, 3) contained reliable spike transmission between excitatory neurons (expediently called IpST herein) and precise sequences of multineuronal spikes, 4) changed its internal state in response to the stimulation of single neurons, and 5) configured a stable pattern of spiking as a whole ("attractor"). Importantly, these features are similar to those found in the cortex in vivo. We describe these 5 features in the following sections.

Sparse Spiking

In the self-sustained state (Fig. 5*A*), the mean firing rates of excitatory and inhibitory neurons are about 0.3 and 5 Hz, respectively (calculated from a 120-min long data set). This infrequency of spontaneous spiking is consistent with electrophysiological reports obtained using patch-clamp recordings from neocortical layer II/III neurons in vivo (Margrie et al. 2002; O'Connor et al. 2010; Minamisawa et al. 2011) and with

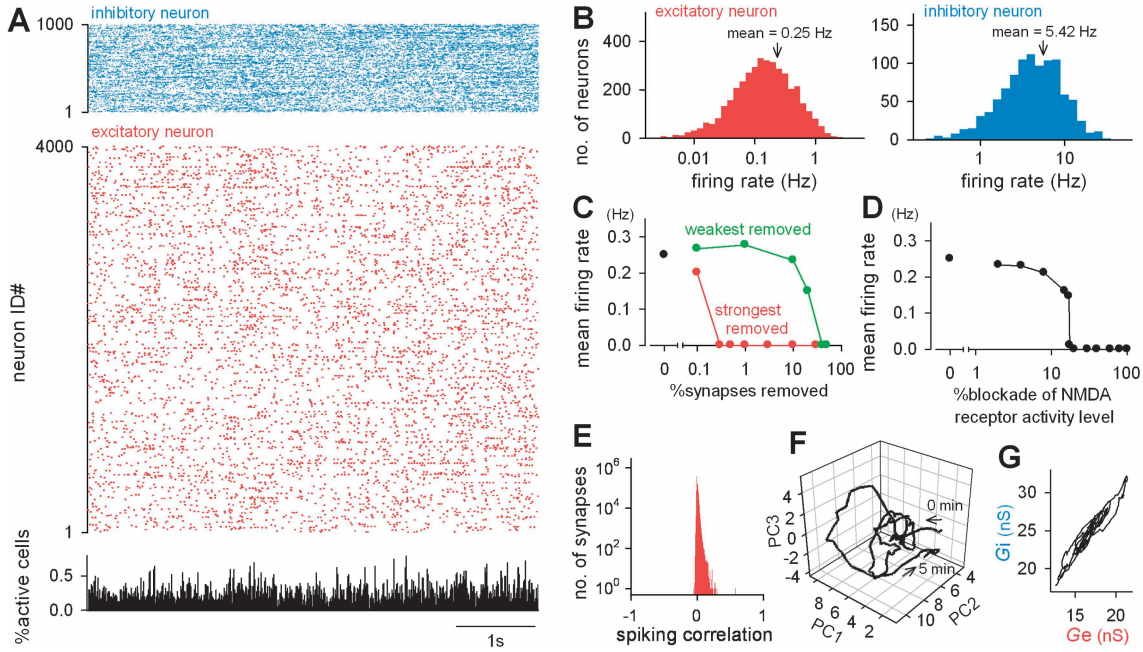

Figure 5. Persistent activity of a recurrent network with strong synapses: simulation. (*A*) Representative spontaneous activity of all 4000 excitatory and 1000 inhibitory neurons in a recurrent network. Bottom histogram represents the number of excitatory neurons activated in a time window of 10 ms. No external noise was required to maintain the network activity. (*B*) Distribution of the frequency of spontaneous spiking emitted by individual excitatory (left) and inhibitory (right) neurons (total 120 min). (*C*) Robustness analysis revealed that removal of the strongest (red) or weakest (green) synapses decreased the mean firing rate of neurons in our network. (*D*) Robustness analysis revealed that reducing the level of NMDA receptor-mediated synaptic conductance decreased the mean firing rate of neurons. (*E*) Histogram of spike count correlation between pairs of 4000 excitatory neurons (total 120 min, 10-ms bin). (*F*) Trajectory of the 3 principal components (PC1, PC2, and PC3) of network activity in a representative data set (5 min). (*G*) Near-linear balance of the net conductance between excitatory (G_e) and inhibitory (G_i) synapses. The 30-s period from the same data as in (*F*) was plotted as function of time.

calcium imaging from CA3 neurons in hippocampal slice cultures (Sasaki et al. 2007; Takahashi et al. 2010). At the single-neuron level, the firing rates varied from neuron to neuron, conforming to a lognormal distribution (Fig. 5*B*; excitatory: $\mu = 10^{-0.82}$ Hz, $\sigma = 10^{0.70}$ Hz, $R = 0.99$, $P < 0.0001$; inhibitory: $\mu = 10^{0.63}$ Hz, $\sigma = 10^{0.60}$ Hz, $R = 0.98$, $P < 0.0001$). This skewed distribution of the spike rates is also consistent with recent evidence in vivo (Hromadka et al. 2008; O'Connor et al. 2010).

We confirmed the importance of the synaptic weight distribution in maintaining spontaneous activity, using 2 tests, 1) a robustness analysis (Fig. 5*C*) and 2) replacement with different distributions (Fig. 6).

First, we conducted a robustness analysis in which an increasing portion of the strongest (or weakest) synapses was removed from the network. Removal of the strongest 0.1% of synapses resulted in a lower frequency of spontaneous firing, and removal of more than 0.3% completely abolished the spiking activity (Fig. 5*C*). Thus, the self-sustained activity is supported by just a small fraction of strong synapses. This result suggests that neural networks can hardly maintain their activity unless embedded with strong synapses. The removal of a small fraction of the weakest synapses did not affect the activity maintenance, but the removal of 30% of these synapses eradicated the activity. Thus, the network activity requires not only infrequent inputs from strong synapses but also massive synaptic bombardment from many weak synapses. This conclusion may not be surprising, as the strongest synapses in our network induce a depolarization of about 10 mV, but the 10-mV depolarization is still smaller than the spike threshold. Therefore, many weak synapses are required to provide depolarizing background noise that helps strong synapse-driven depolarizations to reach the spike threshold. This noise-induced signal enhancement parallels the concept of stochastic resonance (Douglass et al. 1993).

Second, we changed either the mean synaptic weight μ or the SD σ of the lognormal distribution of excitatory-to-excitatory synaptic weights (Fig. 6*A*) and examined the mean firing rates of self-sustained activity in these networks; note that the experimentally obtained μ and σ were 0.47 and 0.44 nS, respectively (Fig. 1*A*). Infrequent spontaneous firing (<2 Hz) was maintained in relatively broad ranges of μ and σ values, although the networks failed to maintain spontaneous activity when either μ or σ was too small, and it exploded into an epileptiform state when either μ or σ was too large, respectively. That is, at σ = 0.44 nS, μ could range from 0.1 to 0.6 (Fig. 6*B*) and at μ = 0.47 nS, σ could range from 0.4 to 1.5 (Fig. 6*C*). Incidentally, the mean firing rate in the epileptiform state was about 30 Hz, the maximal rate allowed in our integrate-and-fire neurons, indicating that virtually all neurons fired at the maximal rate.

The same parameter analysis was conducted for Gaussian distributions of excitatory synaptic weights (Fig. 6*D*). The Gaussian network at the default values of μ = 0.47 nS and σ = 0.44 nS failed to maintain spontaneous activity (Fig. 6*E*,*F*). Therefore, we increased the μ value until the network could maintain the persistent activity, by fixing σ = 0.44 nS (Fig. 6*E*). The activity persisted at μ > about 0.5 nS; however, at >0.8 nS, the mean firing rate jumped to about 30 Hz. Thus, the Gaussian distribution of synaptic weights could maintain infrequent network activity only in a narrow range of μ. Similarly, at μ = 0.47 nS, infrequent network activity was observed at σ values between 0.5 and 1 nS (Fig. 6*F*).

Why is the lognormal distribution less sensitive to changes in the parameters in terms of stabilizing infrequent network

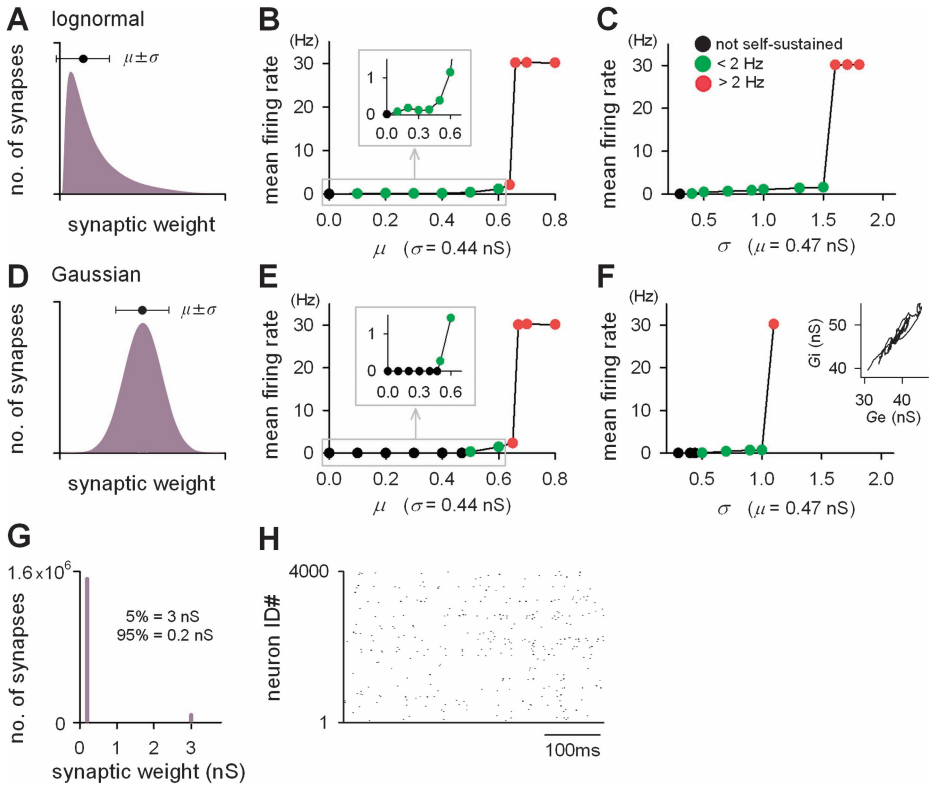

Figure 6. Effects of the distribution shapes of synaptic weights on self-sustained activity: simulation. (*A–F*) The distributions of excitatory synaptic weights were set to be lognormal (*A–C*) or Gaussian (*D–F*) with varying means (μ) and SDs (σ) of synaptic weights. The mean spike frequency of excitatory neurons was plotted against various μ values at a constant σ value of 0.44 nS (*B,E*) and against various σ values at a constant μ value of 0.47 nS (*C,F*). Red, green, and black circles indicate the mean spike frequency of more than 2 Hz, less than 2 Hz, and 0 Hz, respectively. The inset in the panel *F* indicates a time-dependent change in the net conductance between excitatory (G_e) and inhibitory (G_i) synapses in a Gaussian network at μ = 0.5 nS and σ = 0.5 nS. (*G,H*) One simplest example of a network that can self-sustain ongoing activity, in which 5% of excitatory synapses were set at 3 nS and the remaining 95% were at 0.2nS (*G*). This network spontaneously emitted infrequent activities (*H*).

activity? A simple possibility is an extremely inhomogeneous distribution of synaptic weights with a small fraction of synapses generating very large EPSGs. To examine whether the presence of a few strong synapses and many other weak synapses, rather than a lognormal distribution of synaptic weights, is enough to maintain infrequently persistent activity, we tested an extreme case in which 5% of excitatory synapses were at 3 nS and the remaining 95% were 0.2 nS (Fig. 6*G*). We found that this simplified network could maintain infrequent spikes (Fig. 6*H*). Therefore, a key feature required to maintain infrequent activity seems to be a highly inhomogeneous distribution of synaptic weights.

The maintenance of cortical recurrent network activity is known to require NMDA receptors (Metherate and Cruikshank 1999; Buonomano 2003). To investigate the role of NMDA receptors in our network activity, we reduced NMDA receptor-mediated conductance at excitatory synapses, as if the network was treated with a competitive NMDA receptor antagonist at increasing concentrations (Fig. 5*D*). The level of spontaneous activity decreased with the level of NMDA receptor blockade and eventually reached no activity at 30% blockade.

Another distinctive characteristic of the self-sustained activity is asynchronicity, which is also a feature of neocortical activity in vivo (Ecker et al. 2010; Renart et al. 2010). We computed the correlation coefficients between the spike trains of all possible pairs of the 4000 excitatory neurons (n = 7 998 000 pairs, bin = 10 ms). The distribution of the correlation coefficients peaked at zero (Fig. 5*E*), indicating that spontaneous activity is largely asynchronous among individual neurons. To further evaluate the degree of asynchronicity, we calculated the asynchrony index, which is the Shannon entropy normalized to a range between 0 and 1, with higher values representing states that are more asynchronous (Usami et al. 2008; Ujita et al. 2011). The asynchrony index of the spontaneous activity in our network was 0.98, confirming that the activity is nearly completely asynchronous.

Excitation–Inhibition Balance

While the network remained in a steady state, the sets of active neurons at a given moment varied as a function of time, which indicates that the internal state of the network fluctuated dynamically. To depict these microscopic dynamics, we obtained a time series of vectors that represented a set of active neurons during a period of 2 s and compressed the vector dimension using a principal component analysis (Sasaki et al. 2007). The time evolution of the vectors in the principal component space revealed that the network state drifted gradually (Fig. 5*F*), which indicates that active neuron populations vary over time. Interestingly, during these microscopic fluctuations, the entire network maintained the instantaneous balance between excitation and inhibition; the total excitatory and inhibitory synaptic conductances in the network were proportional to each other, whereas the total conductance per se fluctuated as a function of time (Fig. 5*G*). Interestingly, similar balanced fluctuations were observed in excitation and inhibition of infrequent activity that was

maintained in a Gaussian network with $\mu = 0.5$ nS and $\sigma = 0.5$ nS (Fig. 6*F* "inset"). Therefore, the excitation and inhibition balance is not a feature of lognormal networks per se, but it may be rooted in self-sustained network activity.

With respect to the balanced excitation and inhibition, we next examined the effect of network architectures on infrequent network activity. We changed the number of inhibitory neurons and the network connectivity. Our default network contained 4000 excitatory and 1000 inhibitory neurons and had a 10% connection probability between pairs of 5000 neurons. Thus, we changed the number of inhibitory neurons in a range between 100 and 2000 without changing the number of excitatory neurons. We also changed the connection probability in a range between 1% and 100%. The mean firing rates are plotted as a dual function of these 2 parameters (Fig. 7). Infrequently activity was maintained in a wide range of these parameters, that is, 200–2000 inhibitory neurons and 2–50% connectivity, depending on the parameter combinations.

IpST and Spike Sequences

To evaluate the IpST, we plotted peri-presynaptic spike time histograms for postsynaptic spikes. In the case of a strong synapse, such as that shown in Figure 8*A* (1.45 nS), the histogram showed a sharp peak in the firing rate, which is a sign of IpST. We thus computed the IpST probability for all 1 600 000 synaptic pairs and plotted their *P* values against their synaptic weights (Fig. 8*B*). In accordance with our experimental data (Figs 2*C* and 3*C*), significant IpST was evident at synapses stronger than about 1 nS. We next computed the mutual information between presynaptic and postsynaptic spike trains. The amount of information carried by individual

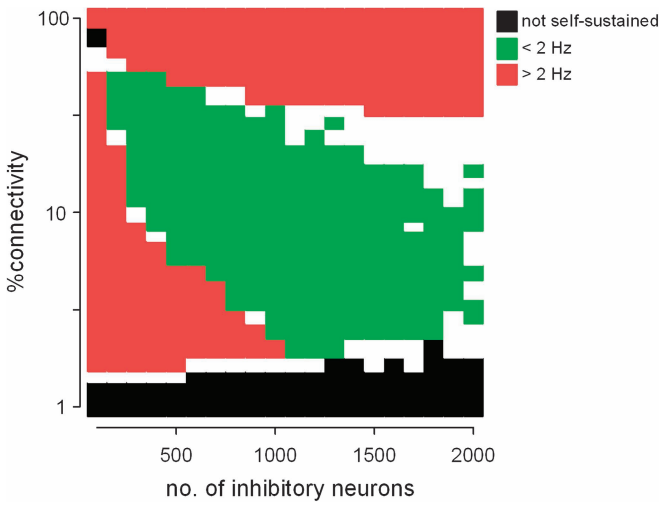

Figure 7. Effects of network architectures on self-sustained activity: simulation. The abscissa indicates the total number of inhibitory neurons in a network. The number of excitatory neurons was 4000 throughout simulation. The ordinate indicates the percentage of interneuronal connectivity. The connectivity density was identical between excitatory-to-excitatory, excitatory-to-inhibitory, inhibitory-to-excitatory, and inhibitory-to-inhibitory connections. For each set of 2 parameters, simulations were repeated using 10—20 different random seeds of network structures and synaptic weights, and the parameter sets that produced consistent results in more than 80% of the trials were indicated by colors; otherwise, they are indicated in white. Red areas indicate parameters that exhibited spontaneous activity at the mean spike frequency of more than 2 Hz, whereas green areas indicate less than 2 Hz. Black areas indicate parameters that could not maintain ongoing activity.

synapses increased with synaptic potency (Fig. 8*C*); the Gini coefficient was 0.83 in the Lorenz curve, and the strongest 10% synapses accounted for about 77% of the total network information (Fig. 8*C* inset).

Consistent with the existence of significantly reliable IpST, we often observed sequences of spikes that appeared repetitively across multiple neurons (Fig. 8*D*). We defined a precise firing sequence (PFS) as a chain of spikes of at least 3 different excitatory neurons with fixed delays that repeated at least 3 times (10-ms jitters allowed). PFSs seemed to occur through specific circuit pathways defined by strong synapses; for example, the weights of the 3 synapses responsible for 4-spike PFSs in Figure 8*D* are shown by arrows in Figure 8*B*. The total number of PFSs in a 1-min data set obtained from 20 networks that were executed with different random seeds was compared with the number found in surrogates in which spikes were randomly exchanged among neurons (Ikegaya et al. 2004; Sasaki et al. 2007). For each data set, 100 surrogates were generated. In all 20 data sets, the PFSs found in the original raster plot were more frequent than the chance level estimated for the surrogates (Fig. 8*E*).

Responsiveness to Small Perturbations

The existence of IpST suggests that the network can respond to even a single spike from a single neuron. We examined whether the network activity patterns changed after the addition of an extraspike. In a representative raster plot (Fig. 9*A*), an extraspike (arrow) was found to cause a different spiking pattern compared with the nonperturbed control. The effect of the extraspike was rapidly propagated through the entire network, resulting in bifurcation of the principal component orbit between control and extraspike-added patterns (Fig. 9*B*, bin = 50 ms).

We quantified this rapid effect of the extraspike by computing the Euclidian distance between 2 activity vectors in the original and extraspike-added raster plots (bin = 5 ms). The Euclidian distance increased immediately after the spike addition and stabilized within 100 ms (Fig. 9*C*). We repeated the same extraspike simulation for all excitatory neurons at various timings of network activity. In all >20 000 trials, single spikes induced rapid and persistent increases in the Euclidian distance. The average responses of all 4000 excitatory neurons demonstrate that the network is sensitive enough to largely change its spiking pattern in response to a small external perturbation (Fig. 9*D*); note that the mean maximal Euclidian distance was about 5, due to the bin size for the Euclidian distance and the network activity frequency.

Macroscopic Stability Against Perturbations

In the above extraspike simulations, we noticed that the level of the entire network activity was maintained, even though the spiking pattern was fully changed after the spike addition. To examine the stability of the self-sustained activity, we applied stronger perturbations by adding or removing spikes for multiple neurons. The altered levels of network activity were found to spontaneously revert to the steady state of infrequent and asynchronous spiking (Fig. 10*A*).

We thus sought to elucidate the robustness of the network activity more comprehensively. We forced the network activity pattern into various configurations and monitored its spontaneous recovery. This network state was defined by the mean firing rate and the asynchrony index (Fig. 10*B*). The state-space

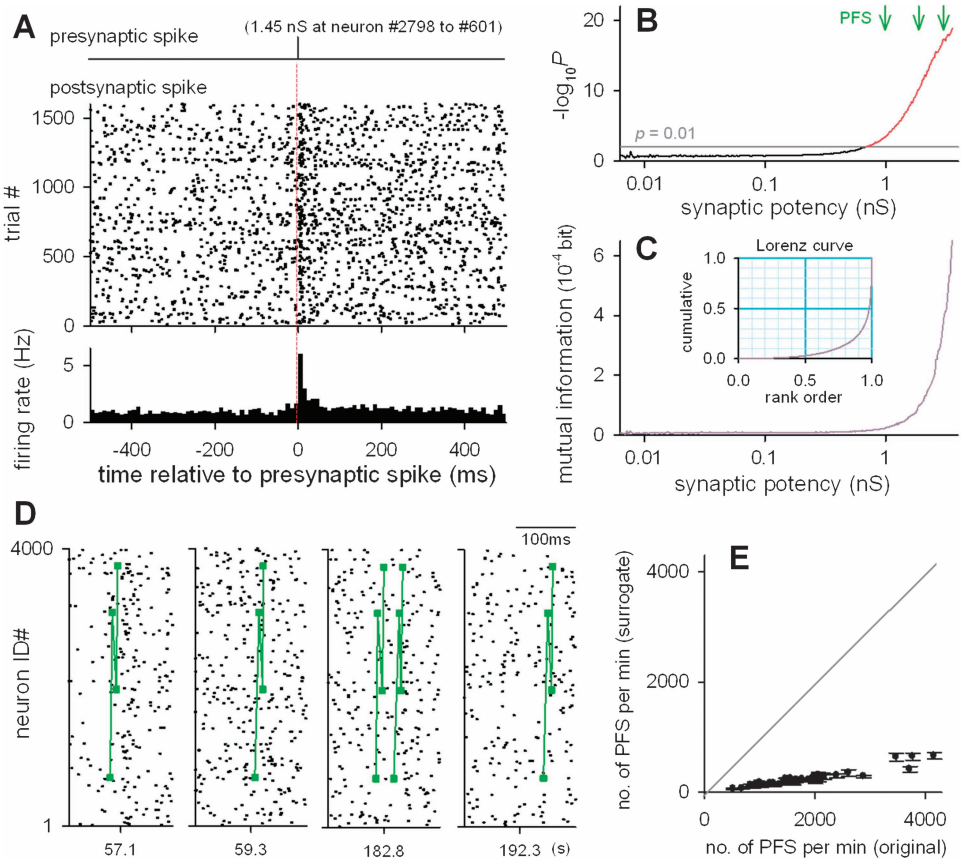

Figure 8. IpST and PFSs in recurrent network activity: simulation. (*A*) Responses of an excitatory postsynaptic neuron (#601) to single spikes from a presynaptic excitatory neuron (#2798) that produced uEPSGs with a potency of 1.45 nS. Top: presynaptic spike timing. Middle: rastergram of postsynaptic spikes. Bottom: peri-presynaptic spike time histogram of postsynaptic spikes. (*B*) *P* values of IpST are plotted against the uEPSG potency. Red lines indicate $P < 0.01$. Arrows indicate the weights of 3 synapses that mediated 4-cell PFSs in (*D*). (*C*) Mutual information (bit per second) between presynaptic and postsynaptic spike trains is plotted against the uEPSG potency. Inset indicates the Lorenz curve of the distribution of mutual information. (*D*) Representative PFSs that consisted of 4 cells and that were repeated 5 times during 200 s. (*E*) Number of PFSs that appeared in the original data sets (abscissa) and in their spike-swapped surrogates (ordinate). Each symbol represents the mean ± SD of 100 surrogates obtained from a single data set ($n = 20$ random seeds).

analysis revealed that the network state was robust against a wide range of external perturbations; the altered network states were drawn into a stable point (attractor) in which the firing rate and the asynchronous index were about 0.3 and >0.9 Hz, respectively. We also found that a network given extremely synchronized spikes was attracted into another "epileptiform" stable point in which the mean firing rate was about 30 Hz. Thus, the state space contained a boundary separating 2 stable points toward which the network was eventually attracted (Fig. 10*B*, green line).

Discussion

We demonstrated that a recurrent network with a long-tailed distribution of synaptic weights exhibited stability and flexibility of activity patterns, both of which are important for brain function. The sparseness and sensitivity of this network activity are in good accordance with recent experimental evidence showing sparse cortical activity in vivo (Margrie et al. 2002; Ecker et al. 2010; O'Connor et al. 2010; Renart et al. 2010; Minamisawa et al. 2011) and high responsiveness to single PCs (Miles and Wong 1983; Brecht et al. 2004; Fujisawa et al. 2006; Houweling and Brecht 2008; Li et al. 2009).

Long-Tailed Distribution of Synaptic Weights

A computational study has shown that spontaneous self-organization of a recurrent neural network through spike timing–dependent plasticity leads to many weak synapses (median synaptic potential amplitude <0.1 mV) and a few synapses that produce >5 mV depolarization (Izhikevich et al. 2004). Moreover, the lognormal distribution of spine sizes is reported to emerge spontaneously when the magnitude of the changes in spine size during synaptic plasticity is proportional to the size of the spine (Loewenstein et al. 2011). Therefore, the long-tailed distribution of synaptic weights is likely a natural consequence of neuronal networks with synaptic plasticity. Consistent with this notion, the long-tailed distribution prevails among synapses in various brain regions that exhibit synaptic plasticity, including the neocortex (Feldmeyer et al. 1999; Song et al. 2005; Lefort et al. 2009), hippocampus (Sayer et al. 1990), and cerebellum (Brunel et al. 2004).

To obtain the uEPSG distribution, we used slice culture preparations rather than acute slice preparations because of the high probability of finding synaptically connected pairs (Takahashi et al. 2010; Sasaki et al. 2011). In acute slices in which more than 80% of the excitatory axons seem to be amputated during slicing (Stepanyants et al. 2009), not only the connection probability but also the true synaptic weights may

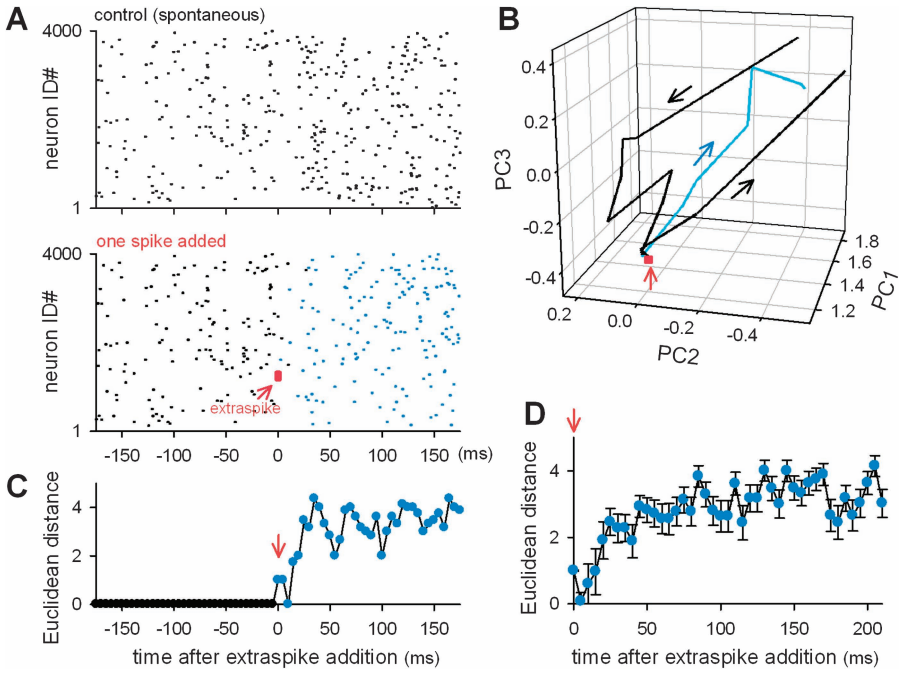

Figure 9. Single spike-induced alternation in the internal state of network activity: simulation. (*A*) Comparison of spontaneous spiking activity between control conditions (top) and conditions under which one extraspike (red) was added at time 0 (bottom). Blue dots indicate spikes different from the control (i.e., perturbed spikes). (*B*) Time evolution in the 3 principal components (PCs) of network activity. Single-spike addition (red arrow) differentiates trajectories between control (black) and extraspike (blue). A period of 800 ms is shown. (*C*) Euclidean distance between spike patterns under conditions with and without an extraspike. Bin = 5 ms. The arrow indicates the time of spike addition. (*D*) Extraspike addition was repeated for all 4000 excitatory neurons, and the mean ± SD of the Euclidean distance was plotted as a function of time.

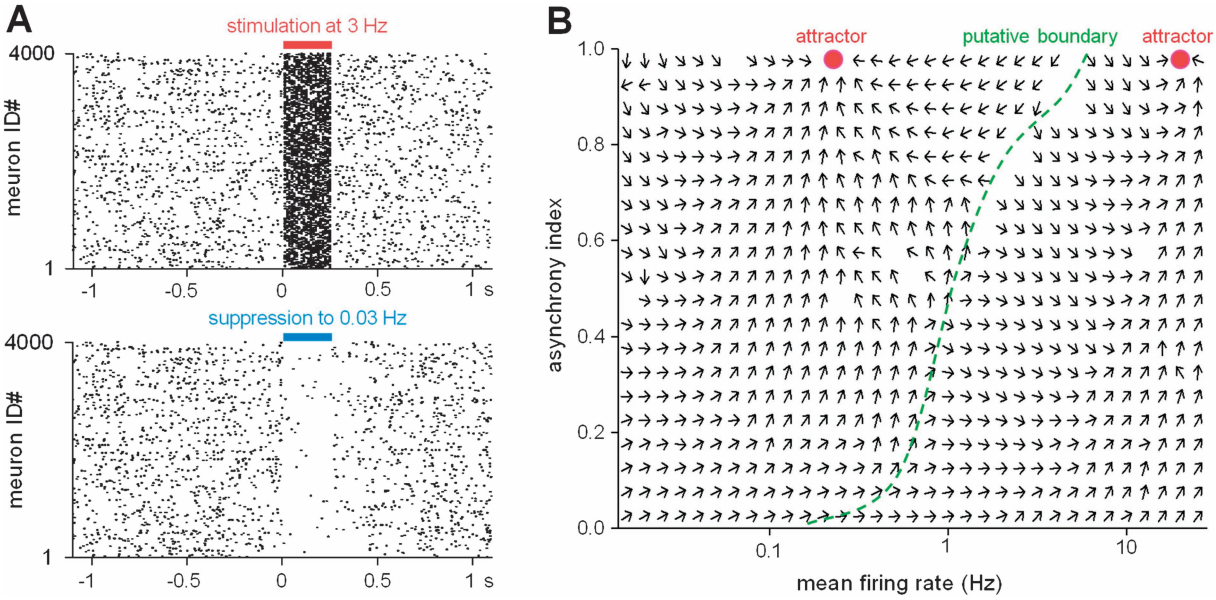

Figure 10. Stability of recurrent network activity: simulation. (*A*) Representative responses of excitatory neurons to spike addition (top, stimulation) and spike removal (left, suppression). Spikes were added or removed so that the mean firing rate became 3 or 0.03 Hz for a period of 250 ms. (*B*) Responses of the network to various levels of 250-ms perturbations (stimulation or suppression) were evaluated in light of the mean firing rate and the asynchrony index. The parameters at a given time were calculated in a time window of 250 ms. The average response changes across 500 trials are indicated by arrows. Arrows are not shown at data points where the network behavior varied among trials with CV of the arrow angle >0.5.

be underestimated because of partial axon lesions; note that synaptic contacts between a single PC pair are often multiple and distributed over postsynaptic dendrites (Markram et al. 1997) and may be partially removed by slicing. Nonetheless, it is noteworthy that the uEPSG potency conformed to a long-tailed distribution with an upper bound of roughly 2 nS in both acute slices (Song et al. 2005; Lefort et al. 2009) and our slice cultures. Therefore, we believe that the IpST seen in our

preparations can be extrapolated to the in vivo brain with little modification.

Interpyramid Spike Transmission (IpST)

In contrast to the theoretical demand of the conventional spike propagation model, the spiking of cortical neurons in vivo is highly asynchronous (Ecker et al. 2010; Renart et al. 2010) and infrequent (Margrie et al. 2002; O'Connor et al. 2010; Minamisawa et al. 2011). Our model study showed that a network provided with large EPSGs can maintain a low network activity level, which implies a critical role for IpST in in vivo-like network activity.

IpST-like phenomena have been suggested by several previous studies. First, in vivo whole-cell patch-clamp studies have demonstrated that the addition of a single extraspike to ongoing activity in a rat barrel cortex induces a transient increase in the firing rates of nearby neurons, which is a sign that a single spike in a PC is propagated to the surrounding network (London et al. 2010). Second, studies using behaving animals have indicated that a small but significant fraction of putative PC pairs exhibits a sharp correlogram peak with a monosynaptic delay (Ts'o et al. 1986; Fujisawa et al. 2008; Quilichini et al. 2010; Takeuchi et al. 2011).

In vitro studies have also suggested the presence of IpST. For example, background synaptic activity enhances the probability that subthreshold inputs elicit spikes (Stacey and Durand 2001; Destexhe et al. 2003; Shu et al. 2003). These studies, however, did not consider the long-tailed uEPSG distribution, and it was unclear whether IpST occurs specifically in a few selected synaptic pathways. We found that IpST was only significant at synapses with amplitudes of more than about 1 nS. Such strong connections composed a very small portion of the total connections. Therefore, in a web of weak PC networks, a few strong connections define stable trajectories through which the majority of neural information flows. Given that a single PC innervates thousands of other PCs in vivo, each PC is expected to have tens of strongly connected postsynaptic targets, which may underlie the unexpectedly potent influence of single PC spiking. In this scheme, weak synapses are thought to provide background noise that modulates the efficiency of IpST by changing the overall activity level and thereby define the network state. Another possibility is that these synapses could offer neuronal networks opportunities for learning and memory because weaker synapses exhibit more capacity for synaptic plasticity (Bi and Poo 1998; Matsuzaki et al. 2004).

The PFSs were rich in spontaneous activity. Because PFSs are likely mediated by IpST, they are not necessarily accompanied by synchronized network activity. Therefore, our PFSs are different from PFSs found in synfire chains, which are theoretically predicted to occur through a feedforward excitatory network (Abeles 1991; Diesmann et al. 1999).

Finally, we speculate that IpST could settle the long-standing debate regarding the dichotomy between 2 neural code hypotheses: the temporal code and the rate code. Large uEPSGs act as "instructive" inputs, and the resultant IpST has a high degree of spike fidelity that favors temporal coding. Small uEPSGs provide "ambient" inputs, and their mass activity level gates IpST, which favors rate coding. Therefore, the temporal and rate code hypotheses may be different perspectives on the same phenomenon.

Funding

This work was supported in part by Grants-in-Aid for Science Research (18021008, 22115003, 22650080, and 22680025) from the Ministry of Education, Culture, Sports, Science and Technology of Japan; the Suzuken Memorial Foundation; the Kanae Foundation for the Promotion of Medical Science; the Daiichi-Sankyo Foundation of Life Science; and the Funding Program for Next Generation World-Leading Researchers (LS023).

Notes

Conflict of Interest : None declared.

References

Abeles M. 1991. Corticonics: neural circuits of the cerebral cortex. vol. xiv. Cambridge (MA): Cambridge University Press. p. 280.

Bi GQ, Poo MM. 1998. Synaptic modifications in cultured hippocampal neurons: dependence on spike timing, synaptic strength, and postsynaptic cell type. J Neurosci. 18:10464–10472.

Brecht M, Schneider M, Sakmann B, Margrie TW. 2004. Whisker movements evoked by stimulation of single pyramidal cells in rat motor cortex. Nature. 427:704–710.

Brunel N, Hakim V, Isope P, Nadal JP, Barbour B. 2004. Optimal information storage and the distribution of synaptic weights: perceptron versus Purkinje cell. Neuron. 43:745–757.

Buonomano DV. 2003. Timing of neural responses in cortical organotypic slices. Proc Natl Acad Sci U S A. 100:4897–4902.

Dayan P, Abbott LF. 2001. Theoretical neuroscience: computational and mathematical modeling of neural systems. Cambridge (MA): Massachusetts Institute of Technology Press.

Destexhe A, Rudolph M, Pare D. 2003. The high-conductance state of neocortical neurons in vivo. Nat Rev Neurosci. 4:739–751.

Diba K, Buzsaki G. 2007. Forward and reverse hippocampal place-cell sequences during ripples. Nat Neurosci. 10:1241–1242.

Diesmann M, Gewaltig MO, Aertsen A. 1999. Stable propagation of synchronous spiking in cortical neural networks. Nature. 402:529–533.

Douglass JK, Wilkens L, Pantazelou E, Moss F. 1993. Noise enhancement of information transfer in crayfish mechanoreceptors by stochastic resonance. Nature. 365:337–340.

Ecker AS, Berens P, Keliris GA, Bethge M, Logothetis NK, Tolias AS. 2010. Decorrelated neuronal firing in cortical microcircuits. Science. 327:584–587.

Feldmeyer D, Egger V, Lubke J, Sakmann B. 1999. Reliable synaptic connections between pairs of excitatory layer 4 neurones within a single 'barrel' of developing rat somatosensory cortex. J Physiol. 521:169–190.

Foster DJ, Wilson MA. 2006. Reverse replay of behavioural sequences in hippocampal place cells during the awake state. Nature. 440:680–683.

Fujisawa S, Amarasingham A, Harrison MT, Buzsaki G. 2008. Behavior-dependent short-term assembly dynamics in the medial prefrontal cortex. Nat Neurosci. 11:823–833.

Fujisawa S, Matsuki N, Ikegaya Y. 2006. Single neurons can induce phase transitions of cortical recurrent networks with multiple internal states. Cereb Cortex. 16:639–654.

Goutagny R, Jackson J, Williams S. 2009. Self-generated theta oscillations in the hippocampus. Nat Neurosci. 12:1491–1493.

Houweling AR, Brecht M. 2008. Behavioural report of single neuron stimulation in somatosensory cortex. Nature. 451:65–68.

Hromadka T, Deweese MR, Zador AM. 2008. Sparse representation of sounds in the unanesthetized auditory cortex. PLoS Biol. 6:e16.

Ikegaya Y, Aaron G, Cossart R, Aronov D, Lampl I, Ferster D, Yuste R. 2004. Synfire chains and cortical songs: temporal modules of cortical activity. Science. 304:559–564.

Izhikevich EM, Gally JA, Edelman GM. 2004. Spike-timing dynamics of neuronal groups. Cereb Cortex. 14:933–944.

Jahr CE, Stevens CF. 1990. Voltage dependence of NMDA-activated macroscopic conductances predicted by single-channel kinetics. J Neurosci. 10:3178–3182.
Kendall MG, Stuart A, Ord JK, Arnold SF, O'Hagan A. 1994. Kendall's advanced theory of statistics. New York: Halsted Press.
Kimura R, Kang S, Takahashi N, Usami A, Matsuki N, Fukai T, Ikegaya Y. 2011. Hippocampal polysynaptic computation. J Neurosci. 31:13168–13179.
Koyama R, Muramatsu R, Sasaki T, Kimura R, Ueyama C, Tamura M, Tamura N, Ichikawa J, Takahashi N, Usami A, et al. 2007. A low-cost method for brain slice cultures. J Pharmacol Sci. 104:191–194.
Lee AK, Wilson MA. 2002. Memory of sequential experience in the hippocampus during slow wave sleep. Neuron. 36:1183–1194.
Lefort S, Tomm C, Floyd Sarria JC, Petersen CC. 2009. The excitatory neuronal network of the C2 barrel column in mouse primary somatosensory cortex. Neuron. 61:301–316.
Lennie P. 2003. The cost of cortical computation. Curr Biol. 13:493–497.
Li CY, Poo MM, Dan Y. 2009. Burst spiking of a single cortical neuron modifies global brain state. Science. 324:643–646.
Liu JK, Buonomano DV. 2009. Embedding multiple trajectories in simulated recurrent neural networks in a self-organizing manner. J Neurosci. 29:13172–13181.
Loewenstein Y, Kuras Y, Rumpel S. 2011. Multiplicative dynamics underlie the emergence of the log-normal distribution of spine sizes in the neocortex in vivo. J Neurosci. 31:59481–59488.
London M, Roth A, Beeren L, Hausser M, Latham PE. 2010. Sensitivity to perturbations in vivo implies high noise and suggests rate coding in cortex. Nature. 466:123–127.
Margrie TW, Brecht M, Sakmann B. 2002. In vivo, low-resistance, whole-cell recordings from neurons in the anaesthetized and awake mammalian brain. Pflugers Arch. 444:491–498.
Markram H, Lubke J, Frotscher M, Roth A, Sakmann B. 1997. Physiology and anatomy of synaptic connections between thick tufted pyramidal neurones in the developing rat neocortex. J Physiol. 500:409–440.
Markram H, Wang Y, Tsodyks M. 1998. Differential signaling via the same axon of neocortical pyramidal neurons. Proc Natl Acad Sci U S A. 95:5323–5328.
Matsuzaki M, Ellis-Davies GC, Nemoto T, Miyashita Y, Iino M, Kasai H. 2001. Dendritic spine geometry is critical for AMPA receptor expression in hippocampal CA1 pyramidal neurons. Nat Neurosci. 4:1086–1092.
Matsuzaki M, Honkura N, Ellis-Davies GC, Kasai H. 2004. Structural basis of long-term potentiation in single dendritic spines. Nature. 429:61–766.
Metherate R, Cruikshank SJ. 1999. Thalamocortical inputs trigger a propagating envelope of gamma-band activity in auditory cortex in vitro. Exp Brain Res. 126:160–174.
Miles R, Wong RK. 1983. Single neurones can initiate synchronized population discharge in the hippocampus. Nature. 306:371–373.
Minamisawa G, Funayama K, Matsuki N, Ikegaya Y. 2011. Intact internal dynamics of the neocortex in acutely paralyzed mice. J Physiol Sci. 61:343–348.
O'Connor DH, Peron SP, Huber D, Svoboda K. 2010. Neural activity in barrel cortex underlying vibrissa-based object localization in mice. Neuron. 67:1048–1061.
Quilichini P, Sirota A, Buzsaki G. 2010. Intrinsic circuit organization and theta-gamma oscillation dynamics in the entorhinal cortex of the rat. J Neurosci. 30:11128–11142.
Renart A, de la Rocha J, Bartho P, Hollender L, Parga N, Reyes A, Harris KD. 2010. The asynchronous state in cortical circuits. Science. 327:587–590.
Reyes AD. 2003. Synchrony-dependent propagation of firing rate in iteratively constructed networks in vitro. Nat Neurosci. 6: 593–599.
Sanchez-Vives MV, McCormick DA. 2000. Cellular and network mechanisms of rhythmic recurrent activity in neocortex. Nat Neurosci. 3:1027–1034.
Sarid L, Bruno R, Sakmann B, Segev I, Feldmeyer D. 2007. Modeling a layer 4-to-layer 2/3 module of a single column in rat neocortex: interweaving in vitro and in vivo experimental observations. Proc Natl Acad Sci U S A. 104:16353–16358.
Sasaki T, Matsuki N, Ikegaya Y. 2007. Metastability of active CA3 networks. J Neurosci. 27:517–528.
Sasaki T, Matsuki N, Ikegaya Y. 2011. Action-potential modulation during axonal conduction. Science. 331:599–601.
Sasaki T, Takahashi N, Matsuki N, Ikegaya Y. 2008. Fast and accurate detection of action potentials from somatic calcium fluctuations. J Neurophysiol. 100:1668–1676.
Sayer RJ, Friedlander MJ, Redman SJ. 1990. The time course and amplitude of EPSPs evoked at synapses between pairs of CA3/CA1 neurons in the hippocampal slice. J Neurosci. 10:826–836.
Shu Y, Hasenstaub A, Badoual M, Bal T, McCormick DA. 2003. Barrages of synaptic activity control the gain and sensitivity of cortical neurons. J Neurosci. 23:10388–10401.
Song S, Sjostrom PJ, Reigl M, Nelson S, Chklovskii DB. 2005. Highly nonrandom features of synaptic connectivity in local cortical circuits. PLoS Biol. 3:e68.
Sorra KE, Harris KM. 1993. Occurrence and three-dimensional structure of multiple synapses between individual radiatum axons and their target pyramidal cells in hippocampal area CA1. J Neurosci. 13:3736–3748.
Stacey WC, Durand DM. 2001. Synaptic noise improves detection of subthreshold signals in hippocampal CA1 neurons. J Neurophysiol. 86:1104–1112.
Stepanyants A, Martinez LM, Ferecsko AS, Kisvarday ZF. 2009. The fractions of short- and long-range connections in the visual cortex. Proc Natl Acad Sci U S A. 106:3555–3560.
Takahashi N, Oba S, Yukinawa N, Ujita S, Mizunuma M, Matsuki N, Ishii S, Ikegaya Y. 2011. High-speed multineuron calcium imaging using Nipkow-type confocal microscopy. Curr Protoc Neurosci. 2:14.
Takahashi N, Sasaki T, Matsumoto W, Matsuki N, Ikegaya Y. 2010. Circuit topology for synchronizing neurons in spontaneously active networks. Proc Natl Acad Sci U S A. 107:10244–10249.
Takeuchi D, Hirabayashi T, Tamura K, Miyashita Y. 2011. Reversal of interlaminar signal between sensory and memory processing in monkey temporal cortex. Science. 331:1443–1447.
Ts'o DY, Gilbert CD, Wiesel TN. 1986. Relationships between horizontal interactions and functional architecture in cat striate cortex as revealed by cross-correlation analysis. J Neurosci. 6:1160–1170.
Ujita S, Mizunuma M, Matsuki N, Ikegaya Y. 2011. Asynchronously enhanced spiking activity of ischemic neuronal networks. Biol Pharm Bull. 34:764–767.
Usami A, Matsuki N, Ikegaya Y. 2008. Spontaneous plasticity of multineuronal activity patterns in activated hippocampal networks. Neural Plast. 2008:108969.